New Phytologist

Research

Pollen analysis using multispectral imaging flow cytometry and deep learning

Susanne Dunker[1,2], Elena Motivans[2,3,4], Demetra Rakosy[1,2], David Boho[5], Patrick Mäder[5], Thomas Hornick[1,2] and Tiffany M. Knight[2,3,4]

[1]Helmholtz-Centre for Environmental Research – UFZ, Permoserstraße 15, Leipzig 04318, Germany; [2]German Centre for Integrative Biodiversity Research – iDiv, Deutscher Platz 5a, Leipzig 04103, Germany; [3]Helmholtz-Centre for Environmental Research – UFZ, Am Kirchtor 1, Halle (Saale) 06120, Germany; [4]Martin Luther University Halle-Wittenberg, Am Kirchtor 1, Halle (Saale) 06108, Germany; [5]Software Engineering for Safety-Critical Systems Group, Technische Universität Ilmenau, Ilmenau 98693, Germany

Author for correspondence:
Susanne Dunker
Email: susanne.dunker@ufz.de

Received: *25 June 2020*
Accepted: *28 July 2020*

New Phytologist (2021) **229:** 593–606
doi: 10.1111/nph.16882

Key words: convolutional neural networks, deep learning, multispectral imaging flow cytometry, pollen, pollinator, species identification.

Summary

- Pollen identification and quantification are crucial but challenging tasks in addressing a variety of evolutionary and ecological questions (pollination, paleobotany), but also for other fields of research (e.g. allergology, honey analysis or forensics). Researchers are exploring alternative methods to automate these tasks but, for several reasons, manual microscopy is still the gold standard.
- In this study, we present a new method for pollen analysis using multispectral imaging flow cytometry in combination with deep learning. We demonstrate that our method allows fast measurement while delivering high accuracy pollen identification.
- A dataset of 426 876 images depicting pollen from 35 plant species was used to train a convolutional neural network classifier. We found the best-performing classifier to yield a species-averaged accuracy of 96%. Even species that are difficult to differentiate using microscopy could be clearly separated.
- Our approach also allows a detailed determination of morphological pollen traits, such as size, symmetry or structure. Our phylogenetic analyses suggest phylogenetic conservatism in some of these traits. Given a comprehensive pollen reference database, we provide a powerful tool to be used in any pollen study with a need for rapid and accurate species identification, pollen grain quantification and trait extraction of recent pollen.

Introduction

There are many questions in ecology and evolution that require accurate identification and quantification of pollen grains. For example, ecologists are often interested in the effectiveness of different pollinator species in transferring pollen to plant species, the functional role of pollinators in networks (e.g. how generalised or specialised they are); and the integration of new pollinator species into communities (e.g. due to biological invasions, climate-driven range shifts) (Tur *et al.*, 2013; Ballantyne *et al.*, 2015; Thompson & Knight, 2018). Evolutionary biologists, in turn, are interested in using paleo-pollen to reconstruct past communities and climates (Harris, 1963; Marcos *et al.*, 2015; Birks *et al.*, 2016), and to understand the selection pressures pollinators impose on floral plant traits (Lankinen & Larsson, 2009; Moreira-Hernández and Muchhala, 2019). Large-scale ecological and evolutionary studies have been so far most limited by methodological constraints as time-consuming and labour-intensive measurements as well as proneness to misidentification.

Researchers need a methodology that allows the identification as well as the quantification of pollen grains quickly and effectively (Ramalho & Kleinert-Giovannini, 1986; Stillman & Flenley, 1996; Holt & Bennett, 2014; Cornman *et al.*, 2015; Hicks *et al.*, 2016). In the past 20 yr, several attempts to automate the process have been proposed, but there are still substantial limitations hindering their practical application on a large scale. For example, metabarcoding is an emerging tool allowing large quantities of pollen samples to be identified to species level (Cornman *et al.*, 2015; Bell *et al.*, 2017; Smart *et al.*, 2017; Gresty *et al.*, 2018; Macgregor *et al.*, 2019). Metabarcoding uses standardised barcode marker gene regions showing specificity within a species and variability between species (Bell *et al.*, 2016). This method achieves high species identification accuracy with high throughput and is becoming cheaper. Metabarcoding will continue to become even more accurate as vascular plants' genetic information becomes more complete. Nevertheless, researchers still debate whether metabarcoding can adequately quantify the abundance of pollen for each species in a sample (Keller *et al.*, 2015; Smart *et al.*, 2017; Bell *et al.*, 2019). Bell *et al.* (2019) pointed out that pollen metabarcoding data cannot be treated as if they are quantitative, because correlation between the number of sequence reads and the number of visually identified pollen

© 2020 The Authors
New Phytologist © 2020 New Phytologist Trust
This is an open access article under the terms of the Creative Commons Attribution-NonCommercial License, which permits use, distribution and reproduction in any medium, provided the original work is properly cited and is not used for commercial purposes.

grain is only moderate. However, quantifying the relative abundance of pollen is essential for answering many ecological and evolutionary questions, for example about the effectiveness of pollinators to particular plant species (Gyan and Woodell, 1987; Davis, 1997; Bell *et al.*, 2019).

Microscopy is still the gold standard for qualitative and quantitative pollen analysis (Erdtman, 1986; Crompton & Wojtas, 1993; Marcos *et al.*, 2015). Microscopy is based on relatively straightforward and widely accessible sample preparation techniques as acetolysis, placing pollen samples on a slide, (occasionally) staining, counting and identifying pollen grains based on traits, such as pollen grain size, surface structure, number and shape of apertures or exine thickness (Erdtman, 1986). Drawbacks of this approach are the high manual effort and the specialised expertise required, both leading to high costs and time consumption and thus to restrictions in sample throughput (Stillman & Flenley, 1996; Ronneberger *et al.*, 2002; Holt *et al.*, 2011; Marcos *et al.*, 2015). There have been promising steps towards automation of microscopic pollen analysis using slide scanning devices, such as 'Classifynder' (Holt *et al.*, 2011; Holt & Bennett, 2014), 'Airyscan' (Sivaguru *et al.*, 2018), 'SR-SIM' (Sivaguru *et al.*, 2018), and 'BAA500' (Oteros *et al.*, 2015). A recent review of 24 studies using automated pollen analysis showed that only seven of these studies could discriminate between more than 10 species and no study could identify more than 26 (Holt & Bennett, 2014). Since this review, several additional studies have emerged using a combination of microscopy and machine learning (Daood *et al.*, 2016, 2018; Marcos *et al.*, 2015; Oteros *et al.*, 2015; Pedersen *et al.* 2017; Sevillano & Aznarte, 2018; Sevillano *et al.*, 2020), the best of which can identify 46 species with 98% accuracy (Sevillano *et al.*, 2020). Most of these studies did not include congener species, which can be difficult to distinguish from each other. For a summary of the number of species and images, classification techniques and accuracy of these recent studies, see Supporting Information Table S1.

In addition, microscopy with slide scanning is still more time consuming than other technologies, such as flow cytometry (Mach *et al.*, 2010). As an example, the Classifynder instrument processes 10 pollen/min (Holt *et al.*, 2011), while imaging flow cytometry allows a maximum event rate of 2000 particles per second.

Flow cytometric approaches have been used so far to identify pollen based on DNA quantity, scatter, and fluorescence traits (Pan *et al.*, 2004; Dewitte *et al.*, 2009; Moon *et al.*, 2011; Kron & Husband, 2012). Flow cytometry facilitates substantially higher capture rates than manual microscopy, that is pollen grains can be rapidly processed as they pass through a fluid stream. However, the pollen species' scatter and fluorescence properties measured with traditional flow cytometric approaches have been inadequate for differentiating certain species (Tennant *et al.*, 2013). Kron and colleagues (Kron *et al.*, 2014) found that distinguishing pollen species was only possible when traditional flow cytometry was used in combination with microscopy.

In this paper, we present a new method for identifying and counting pollen using automated multispectral imaging flow cytometry in combination with deep learning. This interdisciplinary approach combines the advantages of flow cytometry's high throughput with microscopic imaging, resulting in image capture rates of up to 2000 images per second at ×40 magnification. Single pollen grains are hydrodynamically focused (Fig. 1), and imaged with high resolution charge coupled device (CCD) cameras. For every particle passing the light sources, a brightfield as well as various fluorescence images for several spectral ranges is captured.

Multispectral imaging flow cytometry in combination with deep learning has recently been demonstrated as a tool for phytoplankton identification and quantification (Dunker *et al.*, 2018; Dunker, 2019), allowing algae traits to be described in detail and enabling new research regarding the roles of functional traits in shaping patterns of coexistence and diversity in this important functional group of species (Hofmann *et al.*, 2019). Here, we propose a similar application for pollen, aiming primarily for fast and accurate identification and counting of pollen grains. Many pollen traits related to morphology (e.g. diameter, circularity, symmetry) and fluorescence (e.g. bright detail intensity) can be rapidly measured, some for the first time. Thus, our new method opens up the potential to ask new questions in pollen ecology and evolution. Further, if pollen traits are phylogenetically conserved, this will may allow future studies to identify pollen species that are not in the pollen library to family-level or genus-level, based on their traits.

We sampled pollen from 35 plant species across a range of plant families, including some closely related species, to develop and assess multispectral imaging flow cytometry as a tool for pollination biologists. We asked: (1) How accurate is flow cytometry in combination with machine learning at identifying recent entomophilous pollen from a known reference database, and does this accuracy depend on the sample size of pollen per species and the number of images per spectral channel? and (2) Is there a phylogenetic signal in pollen traits?

Materials and Methods

Plant species

Sampling Pollen samples were collected from plant species occurring in montane meadows in the Apuseni Mountains, Romania (site longitude and latitude: 46.49°N, 22.83°W and 46.50°N, 22.81°W; height above sea level *c.* 1150 m). The meadows are actively managed as extensive hay meadows, are highly diverse, and are active research sites for our ongoing projects on the structure and function of plant–pollinator networks (Bennett *et al.*, 2018). Pollen was sampled at the peak flowering time in the second half of July 2018. Our study focused on a representative subset of locally common to rare species from all angiosperm families present in the meadows (Table 1). Individual plant species were identified in the field using identification keys (Fischer, 2008) and several freshly opened flowers of 1–5 plant species were collected. Flowers were stored and dried in sealed tea-bags, the anthers being subsequently removed with clean tweezers, and transferred to 2 ml Eppendorf tubes. Tubes were stored at −20°C until further analysis.

© 2020 The Authors
New Phytologist © 2020 New Phytologist Trust

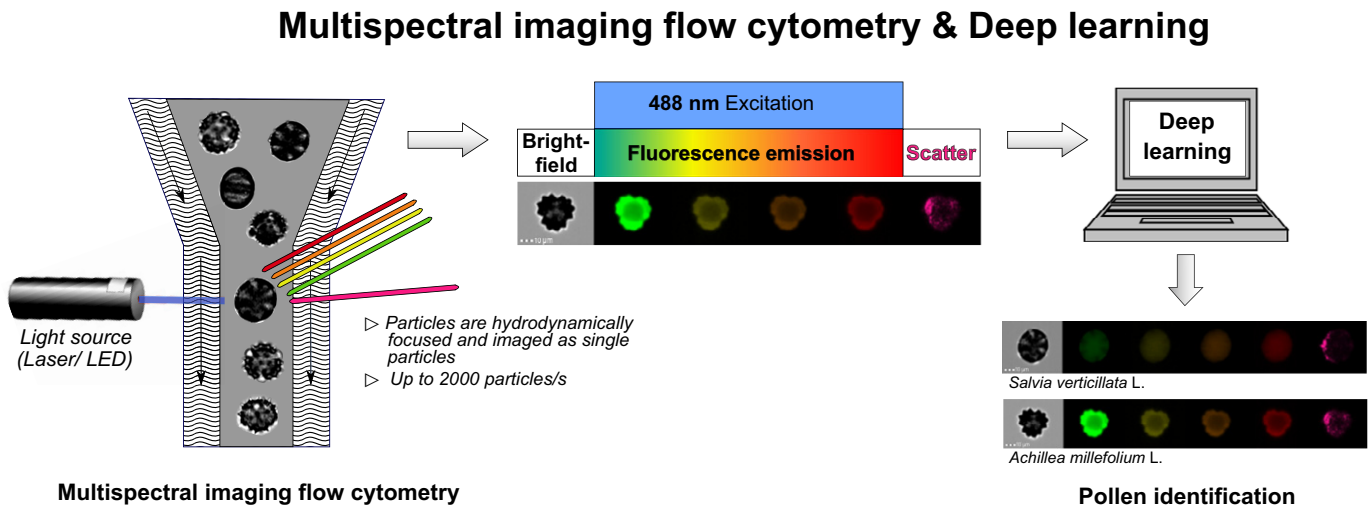

Fig. 1 Schematic workflow of our approach utilising multispectral imaging flow cytometry measurements and deep learning for rapid species identification.

Sample preparation

Depending on the plant species, anthers from 1–5 flowers/species were removed using clean forceps and placed in a 2 ml Eppendorf tube. Pollen isolation buffer (PIB) was prepared according to Aloisi *et al.* (2015) (100 mM K_2HPO_4, pH 7.5; 1 mM EDTA; 0.1% (v/v) Triton X-100) with the modification of using KH_2PO_4 instead of NaH_2PO_4; 500 µl of the buffer was added to each tube. The Eppendorf tubes containing the pollen samples were vortexed and then sonicated for 5 min at room temperature in an ultrasonic bath (Sonorex Digitec DT 514 BH, Bandelin, Berlin, Germany) to separate aggregated pollen grains. Subsequently, the samples were filtered through a 50-µm filter (CellTrics, Sysmex, Norderstedt, Germany) in a 1.5 ml Eppendorf tube and centrifuged for 2 min at 4000 ***g*** (Centrifuge Pico 21, ThermoFisher Scientific, Waltham, MA, USA). The supernatant was carefully discarded and 70 µl of Dulbecco's phosphate buffered saline (without calcium, without magnesium) (Biowest, Nuaillé, France) was added as a standard reagent for flow cytometry to the pellet. If the pollen concentration was low in the final samples, anthers from more flowers were removed with forceps and placed in a 50 ml Falcon tube and processed in the same way as the original samples.

Multispectral imaging flow cytometry

The samples prepared in this way were vortexed before the analysis and measured with an imaging flow cytometer ImageStream®X MK II (Amnis part of Luminex, Austin, Texas, USA) equipped with three lasers (488 m laser with 5 mW intensity, 561 nm laser with 20 mW intensity, and 785 nm laser with 0.1 mW intensity) and two cameras. The instrument is able to simultaneously record a combination of 12 images overall per particle, including one brightfield image and five or six fluorescence images per camera as well as one scatter image on one of the two cameras. The instrument is specifically configured with a non-co-linear spatial arrangement of the two lasers (488 and 561 nm laser) on two different CCD cameras to enable the simultaneous measurement of fluorescence emissions of an identical cell (Patent WO 2019/068352 A 1). The instrument can take images of pollen with a high sampling rate at ×40 magnification with a numeric aperture of 0.75, a pixel size of 0.5 × 0.5 µm and a 60 × 256 µm field of view. As sheath-fluid, Dulbecco's phosphate buffered saline without calcium and magnesium (Biowest, Nuaillé, France) was used. For each pollen suspension prepared as described above, *c.* 50 µl of sample was used per measurement. Data acquisition terminated when 5000 particles were measured or, alternatively, when a time of 25 min had elapsed. We captured all images per defined volume with the instrument-specific Inspire Software (v.200.1.620.1) and processed them with the Ideas software (v.6.2.187.0). Pollen grains were forced by hydrodynamic focusing through an outer core stream of D-PBS, meaning that their orientation was controlled by physical forces and that they adjusted their position in the flow direction, for example prolate and oblate pollen grains mostly adjusted along their longitudinal axis.

Image extraction and gating strategy

Images and respective morphological information are available for 12 different channels; channels 1–6 were captured by the first camera (488 nm laser excitation) and channels 7–12 were captured by the second camera (561 nm laser excitation). Brightfield images were collected on channels 1 and 9; a scatter image was collected on channel 6; and fluorescence images were collected on channel 2 (528/65 nm BP filter), channel 3 (577/35 nm BP filter), channel 4 (610/30 nm BP filter), channel 5 (702/85 nm BP filter), channel 7 (457/45 nm BP filter), channel 8 (537/65 nm BP filter), channel 10 (610/30 nm BP filter), channel 11 (702/85 nm BP filter) and channel 12 (762/35 nm BP filter).

For pollen identification and trait analysis, pollen particles were first separated from nonpollen particles based on threshold

© 2020 The Authors
New Phytologist © 2020 New Phytologist Trust

Table 1 Methodological details for pollen of each plant species.

Family	Plant species	Sample image	No. dataset images (total per channel)	Measurement time (min)	Particle concentration in buffer (pollen ml^{-1})	Pollen size (μm)
Lamiaceae	*Salvia verticillata* L.	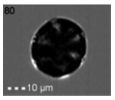	11 892/991	13.3	59 989	30.7 ± 2
	Prunella grandiflora (L.) Scholler	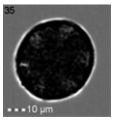	16 152/1346	15.0	71 660	42.2 ± 2
	Thymus pulegioides L.	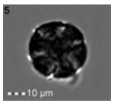	3996/333	24.2	9648	31.5 ± 3
	Stachys officinalis (L.) Trevis	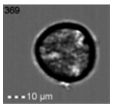	15 816/1318	1.9	543 205	34.0 ± 2
Orobanchaceae	*Euphrasia rostkoviana* Hayne	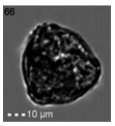	924/77	10.4	5860	40.7 ± 4
Rubiaceae	*Galium verum* L.		16 920/1410	14.0	80 881	17.0 ± 2
Gentianaceae	*Gentianella austriaca* (A. Kern. & Jos. Kern.) Holub	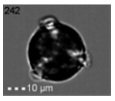	18 228/1519	1.9	641 803	32.6 ± 2
Asteraceae	*Achillea millefolium* L.	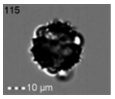	16 392/1366	4.4	248 545	28.3 ± 2
	Achillea distans Willd.	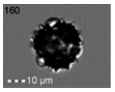	16 236/1353	9.4	116 007	28.7 ± 2
	Leucanthemum vulgare Lam.	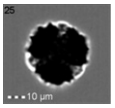	16 716/1393	13.7	79 997	31.7 ± 2
	Leontodon hispidus L.	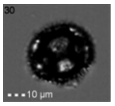	384/32	8.2	2448	34.1 ± 3
	Centaurea jacea	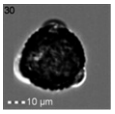	22 032/1836	4.6	321 517	35.2 ± 2
Campanulaceae	*Campanula serrata* (Schult.) Hendrych	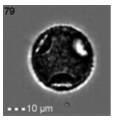	23 928/1994	1.0	1684 996	33.9 ± 2

© 2020 The Authors
New Phytologist © 2020 New Phytologist Trust

Table 1 (Continued)

Family	Plant species	Sample image	No. dataset images (total per channel)	Measurement time (min)	Particle concentration in buffer (pollen ml^{-1})	Pollen size (μm)
	Campanula rotundifolia L.	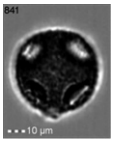	18 504/1542	9.9	121 994	43.9 ± 2
Apiaceae	*Heracleum sphondylium* L.	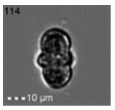	20 148/1679	0.7	2032 718	23.5 ± 2
	Pimpinella major (L.) Huds.	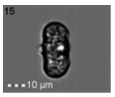	19 992/1666	0.6	2292 523	23.7 ± 2
	Astrantia major L.	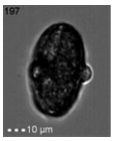	20 808/1734	4.1	341 137	34.9 ± 3
Dipsacaceae	*Scabiosa columbaria*	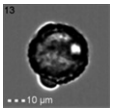	276/23	6.2	543	34.9 ± 3
Primulaceae	*Lysimachia vulgaris* L.	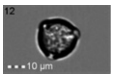	22 704/1892	2.8	549 531	22.5 ± 1
Caryophyllaceae	*Dianthus carthusianorum* L.	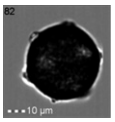	13 548/1129	11.1	80 244	38.5 ± 4
	Stellaria graminea L.	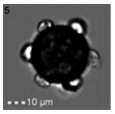	360/30	9.4	2409	32.6 ± 6
Fabaceae	*Trifolium repens* L.	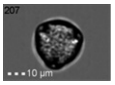	1812/151	8.9	11 849	28.5 ± 2
	Trifolium montanum L.	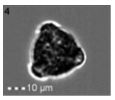	11 700/975	4.2	183 501	27.3 ± 2
	Trifolium pratense L.	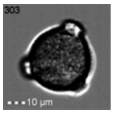	3672/306	10.5	22 893	35.7 ± 4
	Vicia cracca L.	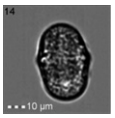	10 692/891	6.2	68 469	33.9 ± 2
	Lotus corniculatus L.	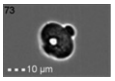	6480/540	25.2	17 152	16.6 ± 2
	Anthyllis vulneraria L.	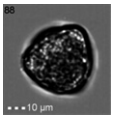	2400/200	9.6	14 110	38.9 ± 3

© 2020 The Authors
New Phytologist © 2020 New Phytologist Trust

Table 1 (Continued)

Family	Plant species	Sample image	No. dataset images (total per channel)	Measurement time (min)	Particle concentration in buffer (pollen ml^{-1})	Pollen size (μm)
	Securigera varia (L.) Lassen	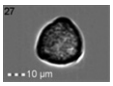	10 668/889	12.0	58 835	25.0 ± 3
Rosaceae	*Potentilla erecta* (L.) Räusch.	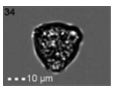	6444/537	11.4	36 697	25.5 ± 1
Violaceae	*Viola tricolour* L.	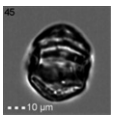	828/69	11.6	3118	35.8 ± 3
Clusiaceae	*Hypericum maculatum* Crantz	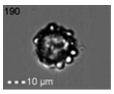	18 672/1556	4.2	296 617	22.2 ± 3
	Hypericum perforatum L.	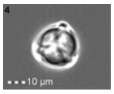	21 756/1813	3.5	415 801	22.5 ± 2
Parnassiaceae	*Parnassia palustris* L.	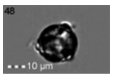	15 180/1265	12.1	84 073	22.5 ± 2
Cistaceae	*Helianthemum nummularium* (L.) Mill.	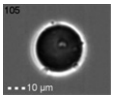	2844/237	17.9	10 515	21.4 ± 6
Ranunculaceae	*Ranunculis acris* L.	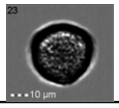	17 772/1481	2.0	609 387	30.1 ± 4.6

This table shows the plant families and species, sorted according to the phylogeny (Figs 3, 4). a representative image taken at ×40 magnification with the imaging flow cytometer, total number and per-channel number of images in the database, measurement time, pollen concentration and averaged pollen size and standard deviation. The number in the top left corner of the image shows the image ID.

levels for brightfield intensities (pollen range: channel 1 = −6300 000 to −63 000/channel 9 = −4000 000 to −50 000). Afterwards, by using circularity (r.u.), single (>11) and nonsingle particles (e.g. doublets) (<11) were distinguished. For trait analysis, only sharp images were used, which could be extracted based on threshold levels of bright detail intensity (channel 9) (354 000–264 000). As a last step, a manual inspection of all collected images was performed in the IDEAS software. All other particles (undefined particles, debris) as well as foreign pollen (all pollen other than the focal species) were excluded based on brightfield images ensuring a high qualitative training dataset. The images were extracted from IDEAS software as 8-bit TIF images for subsequent training of a convolutional neural network.

Deep learning

Dataset Our dataset consisted of 35 573 images for each of the 12 channels covering 35 species and resulting in a total of 426 876 images. This dataset was split into three sets for training, validation, and testing in the proportions 80 : 10 : 10. All images were centre cropped to an equally sized rectangle. In order to gain a more robust and better generalising classifier, the images in the training set were additionally augmented in the following ways: flipped horizontal, flipped vertically, adjusted in brightness ± 12.5%, adjusted in saturation ± 50.0%, adjusted by contrast ± 12.5%, and adjusted in hue ± 20%.

Pollen ID classifier Analysing the captured set of microscopic images poses a computer vision problem and makes convolutional neural networks (CNN) the proper choice of model to train (Nguyen *et al.*, 2018). CNNs are feed-forward artificial neural networks composed of layers with learnable filters. More specifically, an inception network architecture (INCEPTION v.3) with 48 convolution layers was used (Szegedy *et al.*, 2016). In the prestigious ImageNet competition in 2015, this architecture was the first to beat a human performing the same classification task. Transfer learning is a common procedure for training classifiers with fewer than *c.* 1000 000 images (Yosinski *et al.*, 2014). That is, we used a network that was pretrained on the large-scale ImageNet ILSVRC 2012 dataset (http://www.image-net.org/challenges/LSVRC/) before utilising it for our training. The classifiers were trained for 170 epochs (i.e. complete training cycles) with a batch size of 32. The initial learning rate of 0.001 was exponentially decayed every 3 epochs with a factor of 0.94.

© 2020 The Authors
New Phytologist © 2020 New Phytologist Trust

In order to assess the characteristic information conveyed per captured image channel in separation and in complementation to each other, we trained 16 classifiers: classifiers 1–12 assess the individual species characteristics conveyed per channel, while classifiers 13–16 are trained with a mixture of images from three channels each (i.e., 2 + 7 + 9, 2 + 9 + 10, 7 + 9 + 10, 6 + 9 + 12) assessing whether there is complementary information in the channels helpful in generalising and creating a more robust classifier.

Classifier evaluation For the evaluation of the classifier results, different parameters were determined. The classification rate or accuracy for a species is given by the relation:

$$\text{Accuracy} = \frac{\text{TP} + \text{TN}}{\text{TP} + \text{TN} + \text{FP} + \text{FN}}$$

where TP (true positive rate) indicates accurate positive identifications (e.g. pollen species *x* is identified correctly as pollen species *x*) are correctly predicted (pollen *x*), TN (true negative rate) indicates accurate negative identifications (e.g. pollen species *y* is identified correctly as not being pollen species *x*), FP (false positive rate) indicates that the observation is different but predicted as true (e.g. pollen species *y* is identified to be pollen species *x*), and FN (false negative rate) indicates that a true observation is predicted to be different (e.g. pollen species *x* is identified to not be pollen species *x*). As accuracy counts all kinds of errors with the same costs, it is important to consider other more detailed parameters in addition:

$$\text{Recall} = \frac{\text{TP}}{\text{TP} + \text{FN}}$$

High Recall indicates that the species is correctly recognised (a small number of FN).

$$\text{Precision} = \frac{\text{TP}}{\text{TP} + \text{FP}}$$

High Precision indicates that an example labelled as positive is indeed positive (a small number of FP).

To consider both quality parameters equally, the F-measure is calculated based on both, using a harmonic mean value:

$$\text{F-measure} = \frac{2 \times \text{Recall} \times \text{Precision}}{\text{Recall} + \text{Precision}}$$

All tests and evaluations were performed with single-species samples.

Phylogenetic trait analysis and principal component analysis

From the subfraction of manually annotated images, 54 traits (image features) were calculated with the IDEAS software (v.6.2.183.0) for further analyses, including 24 morphological traits, 17 traits characterising pollen grain structure (texture) and 13 fluorescence intensity traits (Table S2). For all traits no raw data, but quality assured data, were used, that is values with higher/lower three standard deviations of the mean value were not considered for the analyses. These traits were selected based on the transferability to classical pollen characteristics (Erdtman, 1986; Beug, 2015). For example, the shape traits 'circularity' and 'aspect ratio' could be translated into equivalents for the pollen form-index (PFormI) (Erdtman, 1986; Beug, 2015), which was determined by the ratio of the length of the polar axis to the equatorial diameter. As an example, pollen with perprolate (PFormI > 2) or prolate shapes (PFormI 1.33-2) show low circularity, whereas pollen with more spheroidal shapes (PFormI 0.75–1.33) show high circularity. Size-related traits include 'area', 'diameter', 'width', 'height', 'length' and 'perimeter'.

To create a phylogeny for our focal plant species, we started with the dated phylogenetic angiosperm supertree created by Zanne *et al.* (2014). If our focal species were not included in the supertree, as was the case for *Campanula serrata*, *Gentianella austriaca* and *Pimpinella major*, they were included in the tree by creating a polytomy with congeners that were present in the tree using the congeneric.merge function from the PEZ package in R (Pearse *et al.*, 2015). We then pruned the supertree to only include our focal species using the drop.tip function from the APE package (Paradis & Schliep, 2019).

Each trait was individually mapped to the phylogeny and tested for phylogenetic signal using Blomberg's K and Pagel's lambda (Münkemüller *et al.*, 2012) with the phylosig function in the PHYTOOLS package (Revell, 2012) (Table S2). As examples, four traits were selected for graphical representation in the main manuscript:
(**1**) The circularity trait is calculated based on the average distance of the object boundary from its centre divided by the variation of this distance. Thus, the closer the object to a circle, the smaller the variation and therefore the trait value will be high and vice versa.
(**2**) The symmetry 2 trait measures the tendency of the object to have a single axis of elongation and therefore two lobes.
(**3**) The symmetry 3 trait measures the tendency of the object to have a three-fold axis of symmetry.
(**4**) Finally, the diameter is defined as $d = 2x\sqrt{\frac{\text{Area}}{\pi}}$.

Three of these traits (circularity, symmetries 2 and 3) showed significant phylogenetic signal and one (diameter) did not. Phylogenetic signals for the rest of the traits can be found in the supplement to this manuscript (Table S1). Those traits are not listed in detail here, as they are common parameters for image analysis (Igathinathane *et al.*, 2008; Zhao *et al.*, 2014; Armi & Fekri-Ershad, 2019). Some of these traits are related to each other and have similar or opposite meanings, for example aspect ratio, elongatedness or symmetry 2.

In addition, to individual traits, a principal component analysis (PCA) was calculated based on a multidimensional resemblance matrix using either all 52 traits (Fig. S2) or only traits that did not include fluorescence intensity (Fig. S1). We tested the first three principal components for a phylogenetic signal using Blomberg's K and Pagel's lambda.

Results

We collected a varying number of reference pollen images per plant species depending on availability. The species with the most images were *Campanula serrata* (23 928 images, 1994 pollen grains), *Hypericum perforatum* (21 756 images, 1813 pollen grains), and *Lysimachia vulgaris* (22 704 images, 1892 pollen

© 2020 The Authors
New Phytologist © 2020 New Phytologist Trust

grains), while *Euphrasia rostkoviana* (924 images, 77 pollen grains), *Leontodon hispidus* (384 images, 32 pollen grains), *Scabiosa columbaria* (276 images, 23 pollen grains), *Stellaria graminea* (360 images, 30 pollen grains) and *Viola tricolour* (828 images, 69 pollen) had the least available images.

Classifier performance

We trained and evaluated various classifiers for single channels as well as for combinations of three channels (cp. Table 2). We found that a model trained on images of one of the two brightfield channels (i.e. channels 1 and 9) performed best in terms of accuracy with a species-averaged accuracy of 95% and 94%, respectively. Species-averaged accuracy means that we first determine the accuracy per species, before averaging across all species. In this way we prevent dominant classes in an unbalanced dataset like ours, that is, some species occur more often than others, to also dominate the overall performance measure. We also found that a model trained on a combination of one brightfield channel (channel 9) and two fluorescence channels (channels 2 and 7) performed best overall with a species-averaged accuracy of 96% and an F-measure of 0.96.

Table 2 Per-channel accuracy and F-measure as indicators for classifier performance for all trained single channel models as well as for the four models trained with multichannel combinations, each including the brightfield channel 9.

	Per-channel accuracy	F-measure
Channel 1	95.17	0.95
Channel 2	85.16	0.87
Channel 3	88.33	0.89
Channel 4	87.52	0.88
Channel 5	83.73	0.84
Channel 6	81.91	0.82
Channel 7	92.74	0.93
Channel 8	89.01	0.89
Channel 9	94.23	0.95
Channel 10	87.89	0.89
Channel 11	89.81	0.89
Channel 12	88.96	0.90
Channel 9-7-2	96.02	0.96
Channel 9-7-10	95.95	0.96
Channel 9-6-12	89.97	0.91
Channel 9-10-2	94.34	0.95

Higher values of per-channel accuracy and F-measure indicate better performance and vice versa.

To understand, how well performance depends on the number of collected pollen images, we plotted the F-measure in relation to the number of collected pollen per species and per family. We found that the required number of images is strongly dependent on the classifier, as for the best multichannel combination, a minimum of 50 images was sufficient to create a classifier of reasonable performance (Fig. 2), even for underrepresented species. By contrast, the worst single channel classifier (channel 5) performed much less reliably and 500-1000 images would be required to have similarly good results as the best multichannel classifier.

With the best multichannel classifier, a confusion matrix was prepared by plotting true vs predicted species identity against each other (Fig. 3). Ideally, true vs predicted species identity should match and result in a 100% overlap visible as only the diagonal SW–NE being coloured in the matrix. Mispredictions were highest for *Scabiosa columbaria*. However, this species had a total of only 23 pollen grains, five of which were used for classifier tests. All other species matched quite well. Congeners of *Achillea, Trifolium*, *Campanula* and *Hypericum* could be robustly identified and, if they were confused, it was not with their congeners, but with species belonging to other genera.

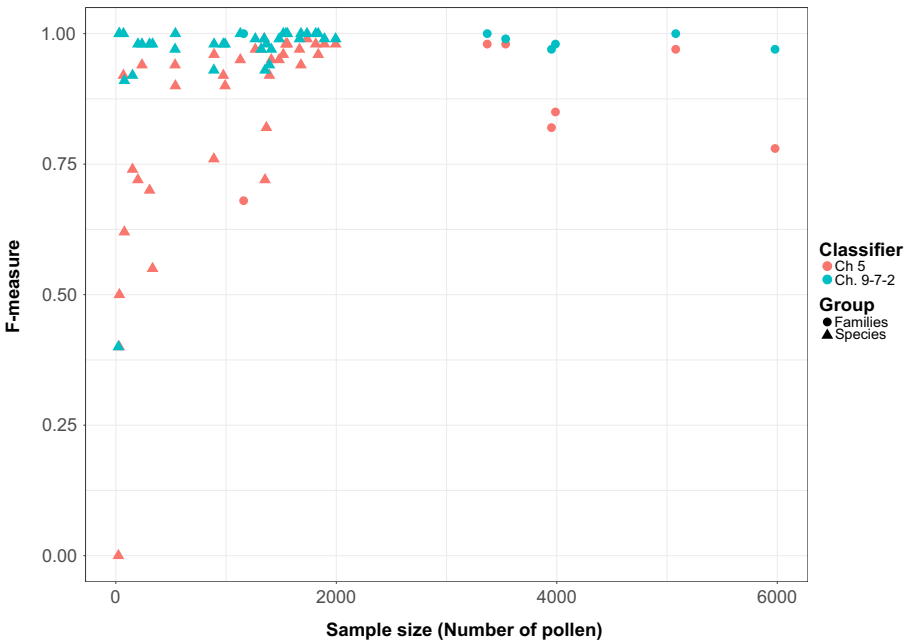

Fig. 2 F-measure for species (triangles) and plant family (circles) level in relation to the number of measured pollen (sample size) available as reference data for the best multichannel classifier (channel 9-7-2 in blue) and the worst single channel classifier (channel 5, red). A high F-measure indicates high values of recall and precision. A detailed version of this figure can be found in the Supporting Information (Fig. S4).

© 2020 The Authors
New Phytologist © 2020 New Phytologist Trust

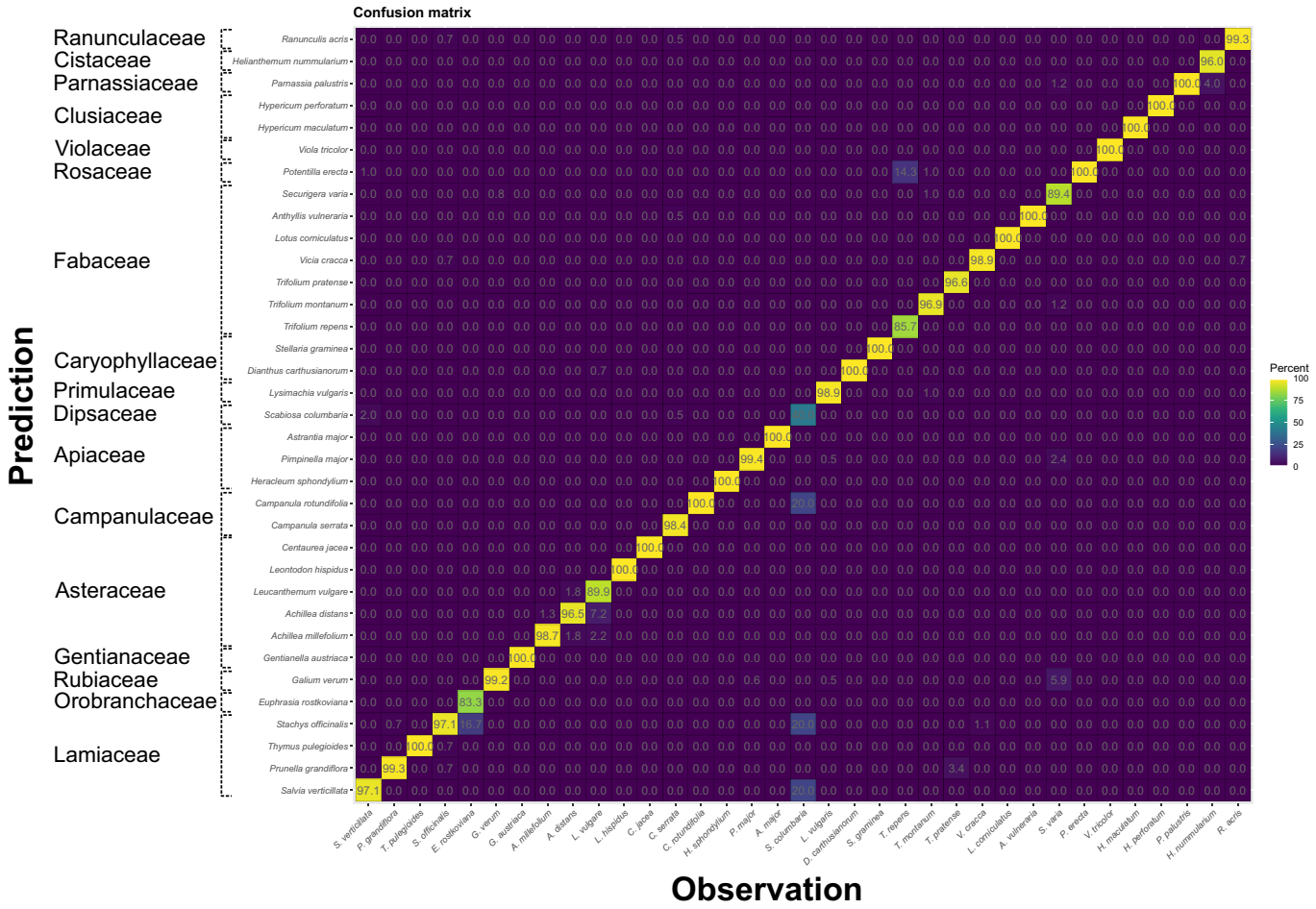

Fig. 3 Confusion matrix for the overall best-performing multichannel classifier combining brightfield images (channel 9) and fluorescence images (channels 2 and 7) showing the match between true and predicted species in percentage.

Phylogenetic signal in traits

For all plant species investigated, various morphological and fluorescence parameters of their pollen grains were derived from respective images, and these traits were tested for phylogenetic signal (Table S2). Twenty-three of the 54 traits had a phylogenetic signal (Table S1). Four traits were considered to display in Fig. 4, three of which had a significant phylogenic signal. This figure highlights that the tricolporate and perprolate/prolate pollen of *Heracleum sphondylium*, *Pimpinella major* and *Astrantia major*, all belonging to Apiaceae, can be easily distinguished from all other groups by high two-dimensional plane dimension (symmetry 2) and lowest roundness (circularity). Campanulaceae species showed the highest circularity and could therefore be well differentiated from other families. The vast majority of species studied had tricolporate pollen such as the Fabaceae *Lotus corniculatus*, *Anthyllis vulneraria* and *Securigera varia*, as well as the Rosaceae *Potentilla erecta* and the Dipsacaceae *Scabiosa columbaria,* showed the highest values in three symmetrical plane dimensions (symmetry 3). The stephanocolpate species, *Salvia verticillata*, *Prunella grandiflora* and *Thymus pulegoides*, belonging to the Lamiaceae, as well as the periporate Caryophyllaceae species *Dianthus carthusianorum* and *Stellaria graminea* revealed lowest symmetry 3.

Interestingly, pollen diameter, an essential trait used in traditional morphological identification of pollen, was found to be more conserved among species belonging to the same genus, but not among genera belonging to the same family. Thus, pollen diameter was similar between the species of the genera *Achillea*, *Campanula*, *Trifolium* and *Hypericum*, but varied markedly between Lamiaceae, Fabaceae and Gentianaceae genera.

Discussion

Imaging flow cytometry in combination with machine learning allows for fast and accurate pollen analyses. In our study, we show that pollen from 35 different plant species across a range of the angiosperm tree of life but also including congeners can be identified with 96% accuracy. This represents a significant technological advance, as most previous studies using feature extraction or CNN have not distinguished among congener species (Marcos *et al.*, 2015; Oteros *et al.*, 2015; Daood *et al.*, 2016, 2018).

In a reasonable time frame of 9 min on average, fast measurements make it easy to rapidly establish a comprehensive image

© 2020 The Authors
New Phytologist © 2020 New Phytologist Trust

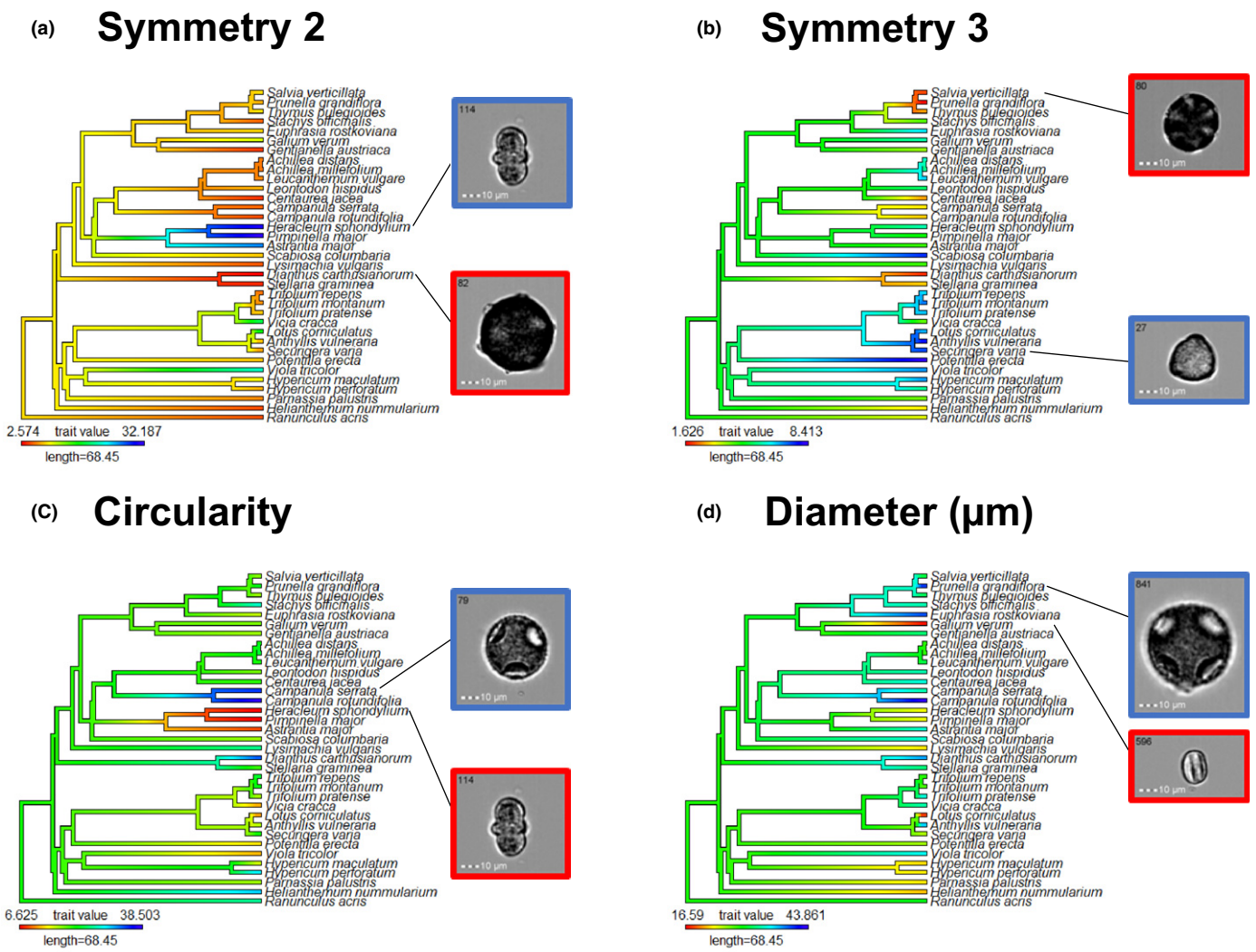

Fig. 4 The phylogeny of investigated plant species, colour coded according to their trait values for (a) biradiate symmetry (symmetry 2), (b) triradiate symmetry (symmetry 3), (c) circularity and (d) diameter. Exemplary pollen images illustrate the differences in the respective trait expression.

database for training of deep learning models. Comparable studies used 1060 (Daood *et al.*, 2016), 13 617 images (Pedersen *et al.*, 2017) or 19 500 images (Sevillano *et al.*, 2020), while in our study the CNN classifier was trained with 426 876 images.

We have previously suggested that a minimum of 200 images per species are required for accurate species identification of phytoplankton (Dunker *et al.*, 2018). By contrast, in the present study on pollen, five out of six species with fewer than 200 pollen grains were classified with an accuracy higher than 90%. Based on these findings, we concluded that between 50 and 100 pollen grains represented a reasonable amount of pollen images on a single channel to be included in the reference library.

Although we were able to show with our approach that a high degree of accuracy was achieved, an explanation of misclassification would be, that they are caused by a different orientation of the pollen on the images. As described in the methods section, particles underlie the physical forces of hydrodynamic focus, meaning that their statistical orientation along their longitudinal axis is relatively stable and herewith reproducible, especially for oblate and prolate pollen grains. We checked the reproducibility of this orientation visually, which in our opinion is not a relevant reasonable source of error explaining the misclassifications in our study.

Most studies using machine learning approaches for species recognition rely solely on microscopic brightfield or darkfield images for object identification (Marcos *et al.*, 2015; Pedersen *et al.*, 2017; Khanzhina *et al.*, 2018; Sevillano & Aznarte, 2018; He *et al.*, 2019; Sevillano *et al.*, 2020). An additional advantage of our approach is that brightfield scatter as well as fluorescent images are collected for every particle, allowing quantification of a broader range of particle properties with spatial image resolution. By testing various classifiers, we found that a classifier with a combination of brightfield and fluorescence images performed significantly better than the brightfield channel alone (Fig. S3), indicating that the information content of brightfield and fluorescence images is complementary. As satisfactory accuracy was

© 2020 The Authors
New Phytologist © 2020 New Phytologist Trust

achieved in this study, the number of channels was reduced to three, with the option to use a combination of up to 12 channels for a higher number of species.

Pollen autofluorescence arises mainly from the sporoderm (intine and exine) from proteins, phenolic compounds and flavonoids in the UV range, as well as carotenoids in the visible range we investigated (Stanley & Linskens, 1974; Roshchina, 2003; Pöhlker *et al.*, 2013). This could explain why the highest accuracy was achieved for the multichannel combinations including channel 2 (carotenoid absorption), while the worst single channel 5 revealed an unspecific absorption in the red region (O'Connor *et al.*, 2011). Pollen fluorescence is discussed as having two important ecological functions: UV-light protection (Stanley & Linskens, 1974; Rozema *et al.*, 2001) and animal attraction (Stanley & Linskens, 1974; Mori *et al.*, 2018). Interestingly, we detected exceptionally high fluorescence from *Hypericum* pollen on all channels with 488 nm excitation (Fig. S2). This fluorescence could be caused by hypericin (Roshchina, 2012) and is especially relevant as European *Hypericum* species are known to provide pollen as the sole reward to their pollinators (Willmer, 2011; Woodcock *et al.*, 2014). Therefore, the high fluorescence could be interpreted as a potential attractant for pollinators. As Pöhlker *et al.* (2013) demonstrated, fluorescence emission can differ between pollen grains of the same species and fluorescence intensity increases with pollen age. In our study, all pollen samples were treated similarly (same age class), and we suggest that great care has to be taken when comparing results across studies as fluorescence signals might be influenced by the age and storage of the respective samples. For paleopalynological analyses it was even shown that fluorescence could be a fast indicator to examine qualitative shifts in sediment fluxes (Yeloff & Hunt, 2005).

A marked point of our results is that we could differentiate between closely related species that belong to families challenging to distinguish using classical microscopy such as the Asteraceae, Fabaceae and Clusiaceae. Often, some species from Asteraceae (Jafari & Ghanbarian, 2007) or some other families are so difficult to distinguish that pollen can only be identified to the family or genus level (Beil *et al.*, 2008; Bilisik *et al.*, 2008; Keller *et al.*, 2015). The differentiation of different species of the same genus has rarely been shown with automated image-based methods. Some of the few exceptions are wind-pollinated *Picea* (Punyasena *et al.*, 2012) and some Poaceae species (Mander *et al.*, 2013; Julier *et al.*, 2016). We hypothesise that the ability to distinguish similar species from each other is due to the high number of images used in our study compared with previous studies (Marcos *et al.*, 2015).

If pollen traits are phylogenetically conserved, this could have potential for research projects interested in identifying key evolutionary transitions in angiosperms and could be used as diagnostic character states to identify untrained plant species in a study. Previous studies have demonstrated that morphological pollen traits, such as shape, symmetry and polarity, showed phylogenetic structure (across 64 species in Wortley *et al.*, 2015). Similarly, we found a phylogenetic signal in the morphological trait 'circularity', which indicates how much the pollen deviates from a spheroidal shape class (lower value of circularity). This difference in circularity is best seen by comparing the perprolate or prolate shape of Apiaceae with the more spheroidal shape of Asteraceae and Campanulaceae species in our database. Many dicotyledons are characterised by three symmetrically arranged longitudinal furrows (tricolpate pollen), which is explained by the fact that four cells are formed from one mother cell after two successive divisions and dependent upon whether Fischer's or Garside's rule of division is apparent (Wodehouse, 1929). We also found a phylogenetic signal in symmetry traits and could distinguish families within the tricolporate pollen class (e.g. Apiaceae with high symmetry 2 and Fabaceae and Dipsacaceae with high symmetry 3), and distinguished between families (e.g. stephanocolpate Lamiaceae species and periporate Caryophyllaceae species, which all had low symmetry 3).

While there was a phylogenetic signal, there was also a great deal of variability in pollen traits within families. This suggests that, at this time, the traits we analysed are only partially suitable to successfully identify a pollen that is not already in our pollen library. This is not surprising, as other studies have pointed out that even in families that have highly conserved pollen traits, there are always some deviant species (Klerk & Joosten, 2007). Thus, pollen traits are similar to other plant traits, such as ecophysiological traits (Liu *et al.*, 2015), which are shaped by local environments (Young & Stanton, 1990).

Despite the lack of a strong phylogenetic signal in our analyses, pollen size (i.e. diameter) is an essential trait for traditional pollen identification (Beug, 2015). Our method allows a rapid assessment of the diameter of a high number of pollen grains (>1000) impossible to achieve in reasonable time with traditional manual microscopic approaches. Consequently, by using this approach, it will be possible to accurately account for the amount of variation in this trait associated with ecological and physiological factors as well as evolutionary adaptation of plant–pollinator pairs. Studies on the relationship between pollen size or other morphological features and pollinators are mainly focused on a limited number of taxonomic groups (Taylor & Levin, 1975; Osborn *et al.*, 1991; Harder, 1998) and it would be interesting to establish a more comprehensive study on this aspect, like the one for example performed by Wortley *et al.* (2015) for evolutionary studies on pollen traits. As one example, body hair morphology and hair density of pollinators affect which pollen size and pollen structure an insect can carry. Therefore, pollen grain size and shape should partially depend on the pollinator species group to which a plant is adapted (Davis, 1997). In addition, pollen size was shown to be influenced by nutrient treatments (Young & Stanton, 1990) or ploidy in several plant species (Altmann *et al.*, 1994; Katsiotis & Forsberg, 1995; Srisuwan *et al.*, 2019). Pollen size is also an indicator of ploidy, which has major relevance for plant physiology and plant distributions (Paule *et al.*, 2017). Some of the differences in pollen size observed for our species and the literature might have been caused by varying ploidy, for example for the plant species *Campanula rotundifolia* (Laanei *et al.*, 1983) and *Leucanthemum vulgare* (Marchi *et al.*, 1983) for which different ploidy was described previously. In our study, the pollen size for both species is higher than reported in Beug

© 2020 The Authors
New Phytologist © 2020 New Phytologist Trust

(2015) and could indicate that our populations have a higher ploidy level. However, we note that pollen size could be also affected by different hydration states, but this should not differ in our study as all samples have been treated similarly.

Rapid and accurate identification and quantification of pollen grains either directly from the flowers or from the body of visiting insects opens up numerous opportunities for assessing different aspects of the reproductive biology of plants and their interaction with pollinators. To apply our method to these kinds of studies, as a next step, it is required that mixed samples of various pollen will be predicted with the existing classifiers. These results need also to be validated against the gold standard microscopy.

Once these steps are established, our approach can be explored for a variety of other pollen-related studies such as health-related research about allergenic pollen, honey analysis, forensics or paleobotanical studies and allows more efficient analyses with much more sample throughput than ever before. These applications would require different reference pollen databases, and for paleopalynology a different way of sample preparation (e.g. with acetolysed pollen material). The method could also be a valuable supplementary approach to pollen metabarcoding.

As the cytometer used in this study is quite an expensive piece of equipment it is important for the future to develop more affordable options, but using a similar technical configuration. At the moment it is recommended that such measurements should be performed centrally, for example in core facilities. As our method is expanded, it will facilitate the creation of a more robust database on pollen phenotypes, allowing for new research on the drivers of variation in pollen size and other morphological traits.

Our method allows ecological questions to be asked on a large spatial and temporal scale, for example on the effects of global land use and climate change on plant reproduction and on the relative importance of different pollinator species for maintaining stable plant–pollinator networks.

Acknowledgements

Funding for this research was provided by the iDiv-Flexpool, project nos. 34600830-13 and 34600865-16, and the Helmholtz Association. The patent submission could create a potential conflict of interest, but to date no financial benefit has been accrued from patent submission. Open access funding enabled and organized by Projekt DEAL.

Author contributions

EM and DR identified all the plants, collected all the pollen and prepared them for analysis; SD performed all flow cytometric measurements; SD and TH carried out the analyses of flow cytometric data; EM did the phylogenetic analyses with the support of TK; SD prepared all images for deep learning; DB performed the machine learning with the support of PM; TH prepared the PCA analyses and SD wrote the manuscript with support from all authors. All authors contributed to the final version of the manuscript.

Data availability

The datasets used and/or analysed during the current study are available from the corresponding author on reasonable request.

ORCID

Susanne Dunker https://orcid.org/0000-0001-7276-776X
Thomas Hornick https://orcid.org/0000-0003-0280-9260
Tiffany M. Knight https://orcid.org/0000-0003-0318-1567
Patrick Mäder https://orcid.org/0000-0001-6871-2707
Demetra Rakosy https://orcid.org/0000-0001-8010-4990

References

Aloisi I, Cai G, Tumiatti V, Minarini A, Del Duca S. 2015. Natural polyamines and synthetic analogs modify the growth and the morphology of *Pyrus communis* pollen tubes affecting ROS levels and causing cell death. *Plant Science* **239**: 92–105.

Altmann T, Damm B, Frommer W, Martin T, Morris P, Schweizer D, Willmitzer L, Schmidt R. 1994. Easy determination of ploidy level in *Arabidopsis thaliana* plants by means of pollen size measurement. *Plant Cell Reports* **13**: 652–656.

Armi L, Fekri-Ershad S. 2019. Texture image analysis and texture classification methods – a review. *International Online Journal of Image Processing and Pattern Recognition* **2**: 1–29.

Ballantyne G, Baldock KCR, Willmer PG. 2015. Constructing more informative plant–pollinator networks: visitation and pollen deposition networks in a heathland plant community. *Proceedings of the Royal Society B: Biological Sciences* **282**: 20151130.

Beil M, Horn H, Schwabe A. 2008. Analysis of pollen loads in a wild bee community (Hymenoptera: Apidae) – a method for elucidating habitat use and foraging distances. *Apidologie* **39**: 456–467.

Bell KL, Burgess KS, Botsch JC, Dobbs EK, Read TD, Brosi BJ. 2019. Quantitative and qualitative assessment of pollen DNA metabarcoding using constructed species mixtures. *Molecular Ecology* **28**: 431–455.

Bell KL, Fowler J, Burgess KS, Dobbs EK, Gruenewald D, Lawley B, Morozumi C, Brosi BJ. 2017. Applying pollen DNA metabarcoding to the study of plant–pollinator interactions. *Applications in Plant Sciences* **5**: 1600124.

Bell KL, de Vere N, Keller A, Richardson RT, Gous A, Burgess KS, Brosi BJ. 2016. Pollen DNA barcoding: current applications and future prospects. *Genome* **59**: 629–640.

Bennett JM, Thompson A, Goia I, Feldmann R, Ştefan V, Bogdan A, Rakosy D, Beloiu M, Biro I-B, Bluemel S *et al.* 2018. A review of European studies on pollination networks and pollen limitation, and a case study designed to fill in a gap. *AoB Plants* **10**: ply068.

Beug H-J. 2015. *Leitfaden der Pollenbestimmung für Mitteleuropa und angrenzende Gebiete, 2nd edn.* München, Germany: Verlag Dr. Friedrich Pfeil.

Bilisik A, Cakmak I, Bicakci A, Malyer H. 2008. Seasonal variation of collected pollen loads of honeybees (*Apis mellifera* L. *anatoliaca*). *Grana* **47**: 70–77.

Birks HJ, Birks HH, Ammann B. 2016. The fourth dimension of vegetation. *Science* **354**: 412–413.

Cornman R, Otto CRV, Iwanowicz D, Pettis JS. 2015. Taxonomic characterization of honey bee (*Apis mellifera*) pollen foraging based on non-overlapping paired-end sequencing of nuclear ribosomal loci. *PLoS ONE* **10**: e0145365.

Crompton CW, Wojtas WA. 1993. *Pollen grains of Canadian honey plants.* Ottawa, Canada: Agriculture Canada and Canada Communication Group-Publishing.

Daood A, Ribeiro E, Bush M. 2016. Pollen recognition using multi-layer feature decomposition. In: *FLAIRS conference.* [WWW document] URL https://www.semanticscholar.org/paper/Pollen-Recognition-Using-Multi-Layer-Feature-Da

© 2020 The Authors
New Phytologist © 2020 New Phytologist Trust

ood-Ribeiro/60390746b60cd25fd3dcf8e1ceae779aafbd45cc [accessed 8 Oct 2020].

Daood A, Ribeiro E, Bush M. 2018. Sequential recognition of pollen grain Z-stacks by combining CNN and RNN. In: *FLAIRS conference*. [WWW document] URL https://www.semanticscholar.org/paper/Sequential-Recognition-of-Pollen-Grain-Z-Stacks-by-Daood-Ribeiro/6ec2ed74e151a589149895be77f1b14a0a8c3c0d [accessed 8 Oct 2020].

Davis AR. 1997. Pollination efficiency of insects. In: Shivanna KR, Sawhney VK, eds. *Pollen biotechnology for crop production and improvement*. New York, NY, USA: Cambridge University Press.

Dewitte A, Eeckhaut T, Huylenbroeck J, Van Bockstaele E. 2009. Occurrence of viable unreduced pollen in a Begonia collection. *Euphytica* **168**: 81–94.

Dunker S. 2019. Hidden secrets behind dots: improved phytoplankton taxonomic resolution using high-throughput imaging flow cytometry. *Cytometry Part A* **95**: 854–868.

Dunker S, Boho D, Wäldchen J, Mäder P. 2018. Combining high-throughput imaging flow cytometry and deep learning for efficient species and life-cycle stage identification of phytoplankton. *BMC Ecology* **18**: 1–15.

Erdtman G. 1986. *Pollen morphology and plant taxonomy: angiosperms*. Leiden, Netherlands: Brill Archive.

Fischer MA. 2008. *Exkursionsflora für Österreich, Liechtenstein und Südtirol*. Auflage. der 'Exkursionsflora von Österreich' 1994. Linz, Austria: OÖ Landesmuseum.

Gresty CEA, Clare E, Devey DS, Cowan RS, Csiba L, Malakasi P, Lewis OT, Willis KJ. 2018. Flower preferences and pollen transport networks for cavity-nesting solitary bees: implications for the design of agri-environment schemes. *Ecology and Evolution* **8**: 7574–7587.

Gyan K, Woodell SRJ. 1987. Analysis of insect pollen loads and pollination efficiency of some common insect visitors of four species of woody rosaceae. *Functional Ecology* **1**: 269.

Harder LD. 1998. Pollen-size comparisons among animal-pollinated angiosperms with different pollination characteristics. *Biological Journal of the Linnean Society* **64**: 513–525.

Harris WF. 1963. Paleo-ecological evidence from pollen and spores. *Proceedings of the New Zealand Ecological Society* **10**, 38–44.

He P, Glowacki G, Gkantiragas A. 2019. *Unsupervised representations of pollen in bright-field microscopy*. [WWW document] URL https://arxiv.org/abs/1908.01866 [accessed 8 October 2020].

Hicks DM, Ouvrard P, Baldock KCR, Baude M, Goddard MA, Kunin WE, Mitschunas N, Memmott J, Morse H, Nikolitsi M. 2016. Food for pollinators: quantifying the nectar and pollen resources of urban flower meadows. *PLoS ONE* **11**: e0158117.

Hofmann P, Chatzinotas A, Harpole WS, Dunker S. 2019. Temperature and stoichiometric dependence of phytoplankton traits. *Ecology* **100**: doi: 10.1002/ecy.2875.

Holt K, Allen G, Hodgson R, Marsland S, Flenley J. 2011. Progress towards an automated trainable pollen location and classifier system for use in the palynology laboratory. *Review of Palaeobotany and Palynology* **167**: 175–183.

Holt KA, Bennett KD. 2014. Principles and methods for automated palynology. *New Phytologist* **203**: 735–742.

Igathinathane C, Pordesimo LO, Columbus EP, Batchelor WD, Methuku SR. 2008. Shape identification and particles size distribution from basic shape parameters using ImageJ. *Computers and Electronics in Agriculture* **63**: 168–182.

Jafari E, Ghanbarian GH. 2007. Pollen morphological studies on selected taxa of Asteraceae. *Journal of Plant Sciences* **2**: 195–201.

Julier ACM, Jardine PE, Coe AL, Gosling WD, Lomax BH, Fraser WT. 2016. Chemotaxonomy as a tool for interpreting the cryptic diversity of Poaceae pollen. *Review of Palaeobotany and Palynology* **235**: 140–147.

Katsiotis A, Forsberg RA. 1995. Pollen grain size in four ploidy levels of genusAvena. *Euphytica* **83**: 103–108.

Keller A, Danner N, Grimmer G, Ankenbrand M, von der Ohe K, von der Ohe W, Rost S, Härtel S, Steffan-Dewenter I. 2015. Evaluating multiplexed next-generation sequencing as a method in palynology for mixed pollen samples. *Plant Biology* **17**: 558–566.

Khanzhina N, Putin E, Filchenkov A, Zamyatina E. 2018. Pollen grain recognition using convolutional neural network. In: *European Symposium on Artificial Neural Networks (ESANN)* [WWW document] URL https://www.i6doc.com/en/book/?gcoi=28001100176760 [8 October 2020].

Klerk P, Joosten H 2007. The difference between pollen types and plant taxa: a plea for clarity and scientific freedom. *E&G Quaternary Science Journal* **56**: 162–171.

Kron P, Husband BC. 2012. Using flow cytometry to estimate pollen DNA content: improved methodology and applications. *Annals of Botany* **110**: 1067–1078.

Kron P, Kwok A, Husband BC. 2014. Flow cytometric analysis of pollen grains collected from individual bees provides information about pollen load composition and foraging behaviour. *Annals of Botany* **113**: 191–197.

Laanei MM, Croff B, Wahlstrøm R. 1983. Cytotype distribution in the *Campanula rotundifolia* complex in Norway, and cyto-morphological characteristics of diploid and tetraploid groups. *Hereditas* **99**: 21–48.

Lankinen Å, Larsson MC. 2009. Conflicting selection pressures on reproductive functions and speciation in plants. *Evolutionary Ecology* **23**: 147–157.

Liu H, Xu Q, He P, Santiago LS, Yang K, Ye Q. 2015. Strong phylogenetic signals and phylogenetic niche conservatism in ecophysiological traits across divergent lineages of Magnoliaceae. *Scientific Reports* **5**: 12246.

Macgregor CJ, Kitson JJN, Fox R, Hahn C, Lunt DH, Pocock MJO, Evans DM. 2019. Construction, validation, and application of nocturnal pollen transport networks in an agro-ecosystem: a comparison using light microscopy and DNA metabarcoding. *Ecological Entomology* **44**: 17–29.

Mach WJ, Thimmesch AR, Orr JA, Slusser JG, Pierce JD. 2010. Flow cytometry and laser scanning cytometry, a comparison of techniques. *Journal of Clinical Monitoring and Computing* **24**: 251–259.

Mander L, Li M, Mio W, Fowlkes CC, Punyasena SW. 2013. Classification of grass pollen through the quantitative analysis of surface ornamentation and texture. *Proceedings of the Royal Society B: Biological Sciences* **280**: 20131905.

Marchi P, Illuminati O, Macioce A, Capineri R, D'Amato G. 1983. Genome evolution and polyploidy in *Leucanthemum Vulgare* Lam. Aggr. (Compositae). Karyotype analysis and DNA Microdensitometry. *Caryologia* **36**: 1–18.

Marcos JV, Nava R, Cristóbal G, Redondo R, Escalante-Ramírez B, Bueno G, Déniz Ó, González-Porto A, Pardo C, Chung F, Rodríguez T. 2015. Automated pollen identification using microscopic imaging and texture analysis. *Micron* **68**: 36–46.

Moon HS, Eda S, Saxton AM, Ow DW, Stewart CN. 2011. An efficient and rapid transgenic pollen screening and detection method using flow cytometry. *Biotechnology Journal* **6**: 118–123.

Moreira-Hernández JI, Muchhala N. 2019. Importance of pollinator-mediated interspecific pollen transfer for angiosperm evolution. *Annual Review of Ecology, Evolution, and Systematics* **50**: 191–217.

Mori S, Fukui H, Oishi M, Sakuma M, Kawakami M, Tsukioka J, Goto K, Hirai N. 2018. Biocommunication between plants and pollinating insects through fluorescence of pollen and anthers. *Journal of Chemical Ecology* **44**: 591–600.

Münkemüller T, Lavergne S, Bzeznik B, Dray S, Jombart T, Schiffers K, Thuiller W. 2012. How to measure and test phylogenetic signal. *Methods in Ecology and Evolution* **3**: 743–756.

Nguyen LD, Lin D, Lin Z, Cao J. 2018. Deep CNNs for microscopic image classification by exploiting transfer learning and feature concatenation. In: *2018 IEEE international symposium on circuits and systems (ISCAS)*. Piscataway, NJ, USA: IEEE. doi: 10.1109/iscas.2018.8351550.

O'Connor DJ, Iacopino D, Healy DA, O'Sullivan D, Sodeau JR. 2011. The intrinsic fluorescence spectra of selected pollen and fungal spores. *Atmospheric Environment* **45**: 6451–6458.

Osborn JM, Taylor TN, Schneider EL. 1991. Pollen morphology and ultrastructure of the cabombaceae: correlations with pollination biology. *American Journal of Botany* **78**: 1367–1378.

Oteros J, Pusch G, Weichenmeier I, Heimann U, Möller R, Röseler S, Traidl-Hoffmann C, Schmidt-Weber C, Buters JT. 2015. Automatic and online pollen monitoring. *IAA* **167**: 158–166.

Pan G, Zhou Y, Fowke LC, Wang H. 2004. An efficient method for flow cytometric analysis of pollen and detection of 2 n nuclei in *Brassica napus* pollen. *Plant Cell Reports* **23**: 196–202.

Paradis E, Schliep K. 2019. ape 5.0: an environment for modern phylogenetics and evolutionary analyses in R. *Bioinformatics* **35**: 526–528.

© 2020 The Authors
New Phytologist © 2020 New Phytologist Trust

Paule J, Gregor T, Schmidt M, Gerstner E-M, Dersch G, Dressler S, Wesche K, Zizka G. 2017. Chromosome numbers of the flora of Germany—a new online database of georeferenced chromosome counts and flow cytometric ploidy estimates. *Plant Systematics and Evolution* **303**: 1123–1129.

Pearse WD, Cadotte MW, Cavender-Bares J, Ives AR, Tucker CM, Walker SC, Helmus MR. 2015. pez: phylogenetics for the environmental sciences. *Bioinformatics* **31**: 2888–2890.

Pedersen B, Bailey DG, Hodgson RM, Holt K, Marsland S. 2017. Model and feature selection for the classification of dark field pollen images using the classifynder system. In: *2017 International conference on image and vision computing New Zealand (IVCNZ), 4–6 Dec. 2017*. Piscataway, NJ, USA: IEEE. doi: 10.1109/ivcnz.2017.8402498

Pöhlker C, Huffman JA, Förster J-D, Pöschl U. 2013. Autofluorescence of atmospheric bioaerosols: spectral fingerprints and taxonomic trends of pollen. *Atmospheric Measurement Techniques* **6**: 3369–3392.

Punyasena SW, Tcheng DK, Wesseln C, Mueller PG. 2012. Classifying black and white spruce pollen using layered machine learning. *New Phytologist* **196**: 937–944.

Ramalho M, Kleinert-Giovannini A. 1986. Some aspects of the utilization of pollen analysis in ecological research. *Apidologie* **17**: 159–174.

Revell LJ. 2012. phytools: an R package for phylogenetic comparative biology (and other things). *Methods in Ecology and Evolution* **3**: 217–223.

Ronneberger O, Schultz E, Burkhardt H. 2002. Automated pollen recognition using 3D volume images from fluorescence microscopy. *Aerobiologia* **18**: 107–115.

Roshchina VV. 2003. Autofluorescence of plant secreting cells as a biosensor and bioindicator reaction. *Journal of Fluorescence* **13**: 403–420.

Roshchina VV. 2012. Vital autofluorescence: application to the study of plant living cells. *International Journal of Spectroscopy* **2012**: 1–14.

Rozema J, Broekman RA, Blokker P, Meijkamp BB, de Bakker N, van de Staaij J, van Beem A, Ariese F, Kars SM. 2001. UV-B absorbance and UV-B absorbing compounds (para-coumaric acid) in pollen and sporopollenin: the perspective to track historic UV-B levels. *Journal of Photochemistry and Photobiology B: Biology* **62**: 108–117.

Sevillano V, Aznarte JL. 2018. Improving classification of pollen grain images of the POLEN23E dataset through three different applications of deep learning convolutional neural networks. *PLoS ONE* **13**: e0201807.

Sevillano V, Holt K, Aznarte JL. 2020. Precise automatic classification of 46 different pollen types with convolutional neural networks. *PLoS ONE* **15**: e0229751.

Sivaguru M, Urban MA, Fried G, Wesseln CJ, Mander L, Punyasena SW. 2018. Comparative performance of airyscan and structured illumination superresolution microscopy in the study of the surface texture and 3D shape of pollen. *Microscopy Research and Technique* **81**: 101–114.

Smart MD, Cornman RS, Iwanowicz DD, McDermott-Kubeczko M, Pettis JS, Spivak MS, Otto CRV. 2017. A comparison of honey bee-collected pollen from working agricultural lands using light microscopy and ITS metabarcoding. *Environmental Entomology* **46**: 38–49.

Srisuwan S, Sihachakr D, Martín J, Vallès J, Ressayre A, Brown SC, Siljak-Yakovlev S. 2019. Change in nuclear DNA content and pollen size with polyploidisation in the sweet potato (*Ipomoea batatas*, Convolvulaceae) complex. *Plant Biology* **21**: 237–247.

Stanley RG, Linskens HF. 1974. Pollen pigments. In Stanley RG, Linskens HF, eds. *Pollen. Biology Biochemistry Management*. Berlin/Heidelberg, Germany: Springer, 223–246.

Stillman EC, Flenley JR. 1996. The needs and prospects for automation in palynology. *Quaternary Science Reviews* **15**: 1–5.

Szegedy C, Vanhoucke V, Ioffe S, Shlens J, Wojna Z. 2016. Rethinking the Inception Architecture for Computer Vision. In: *29th IEEE conference on computer vision and pattern recognition, CVPR 2016 proceedings, 26 June–1 July 2016, Las Vegas, Nevada*. With assistance of Bajcsy R, Li F-F, Tuytelaars T. Piscataway, NJ, USA: IEEE. doi: 10.1109/cvpr.2016.308.

Taylor TN, Levin DA. 1975. Pollen morphology of polemoniaceae in relation to systematics and pollination systems: scanning electron microscopy. *Grana* **15**: 92–112.

Tennant RK, Jones R, Brock F, Cook C, Turney C, Love J, Lee R. 2013. A new flow cytometry method enabling rapid purification of fossil pollen from terrestrial sediments for AMS radiocarbon dating. *Journal of Quaternary Science* **28**: 229–236.

Thompson AH, Knight TM. 2018. Exotic plant species receive adequate pollinator service despite variable integration into plant-pollinator networks. *Oecologia* **187**: 135–142.

Tur C, Castro-Urgal R, Traveset A. 2013. Linking plant specialization to dependence in interactions for seed set in pollination networks. *PLoS ONE* **8**: e78294.

Willmer P. 2011. *Pollination and floral ecology*. Princeton University Press.

Wodehouse RP. 1929. The origin of symmetry patterns of pollen grains. *Bulletin of the Torrey Botanical Club* **56**: 339.

Woodcock TS, Larson BMH, Kevan PG, Inouye DW, Lunau K. 2014. Flies and flowers II: floral attractants and rewards. *Journal of Pollination Ecology* **12**: doi: 10.26786/1920-7603(2014)5.

Wortley AH, Wang H, Lu L, Li D-z, Blackmore S. 2015. Evolution of angiosperm pollen. 1. Introduction. *Annals of the Missouri Botanical Garden* **100**: 177–226.

Yeloff D, Hunt C. 2005. Fluorescence microscopy of pollen and spores: a tool for investigating environmental change. *Review of Palaeobotany and Palynology* **133**: 203–219.

Yosinski J, Clune J, Bengio Y, Lipson H. 2014. How transferable are features in deep neural networks? *Advances in Neural Information Processing Systems* **27**: 3320–3328.

Young HJ, Stanton ML. 1990. Influence of environmental quality on pollen competitive ability in wild radish. *Science* **248**: 1631–1633.

Zanne AE, Tank DC, Cornwell WK, Eastman JM, Smith SA, FitzJohn RG, McGlinn DJ, O'Meara BC, Moles AT, Reich PB. 2014. Three keys to the radiation of angiosperms into freezing environments. *Nature* **506**: 89–92.

Zhao Q, Shi C-Z, Luo L-P. 2014. Role of the texture features of images in the diagnosis of solitary pulmonary nodules in different sizes. *Chinese Journal of Cancer Research* **26**: 451–458.

Supporting Information

Additional Supporting Information may be found online in the Supporting Information section at the end of the article.

Fig. S1 Principal component analysis (PCA) of morphological pollen traits (without fluorescence).

Fig. S2 Principal component analysis (PCA) of pollen traits, including morphological and fluorescence traits.

Fig. S3 Multiparameter comparison using the Kruskal–Wallis test for differences of F-measure between channels.

Fig. S4 Detailed version of Fig. 2.

Table S1 Updated literature review based on the publication of Holt and Bennett (2014), covering the published literature from 2014 onwards.

Table S2 List of traits and their phylogenetic signal (*P*-values for Blomberg's K and Pagel's lambda).

Please note: Wiley Blackwell are not responsible for the content or functionality of any Supporting Information supplied by the authors. Any queries (other than missing material) should be directed to the *New Phytologist* Central Office.

© 2020 The Authors
New Phytologist © 2020 New Phytologist Trust

New Phytologist Supporting Information

Pollen analysis using multispectral imaging flow cytometry and deep learning

Susanne Dunker, Elena Motivans, Demetra Rakosy, David Boho, Patrick Mäder, Thomas Hornick, Tiffany M. Knight

Article acceptance date: 28 July 2020.

Supplemental Figures

Fig. S1: Principal component analysis (PCA) of morphological pollen traits (without fluorescence).

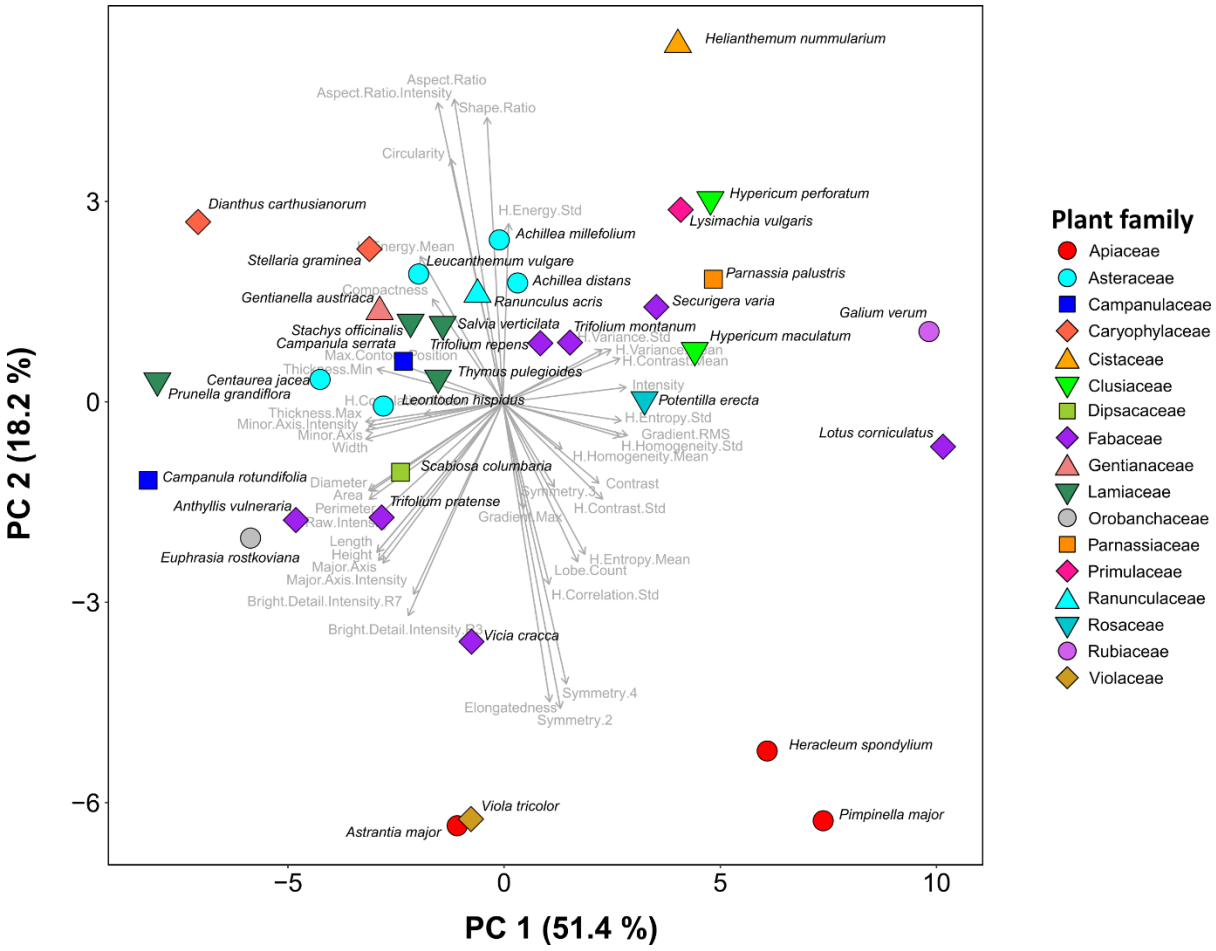

Fig. S2: Principal component analysis (PCA) of pollen traits, including morphological and fluorescence traits.

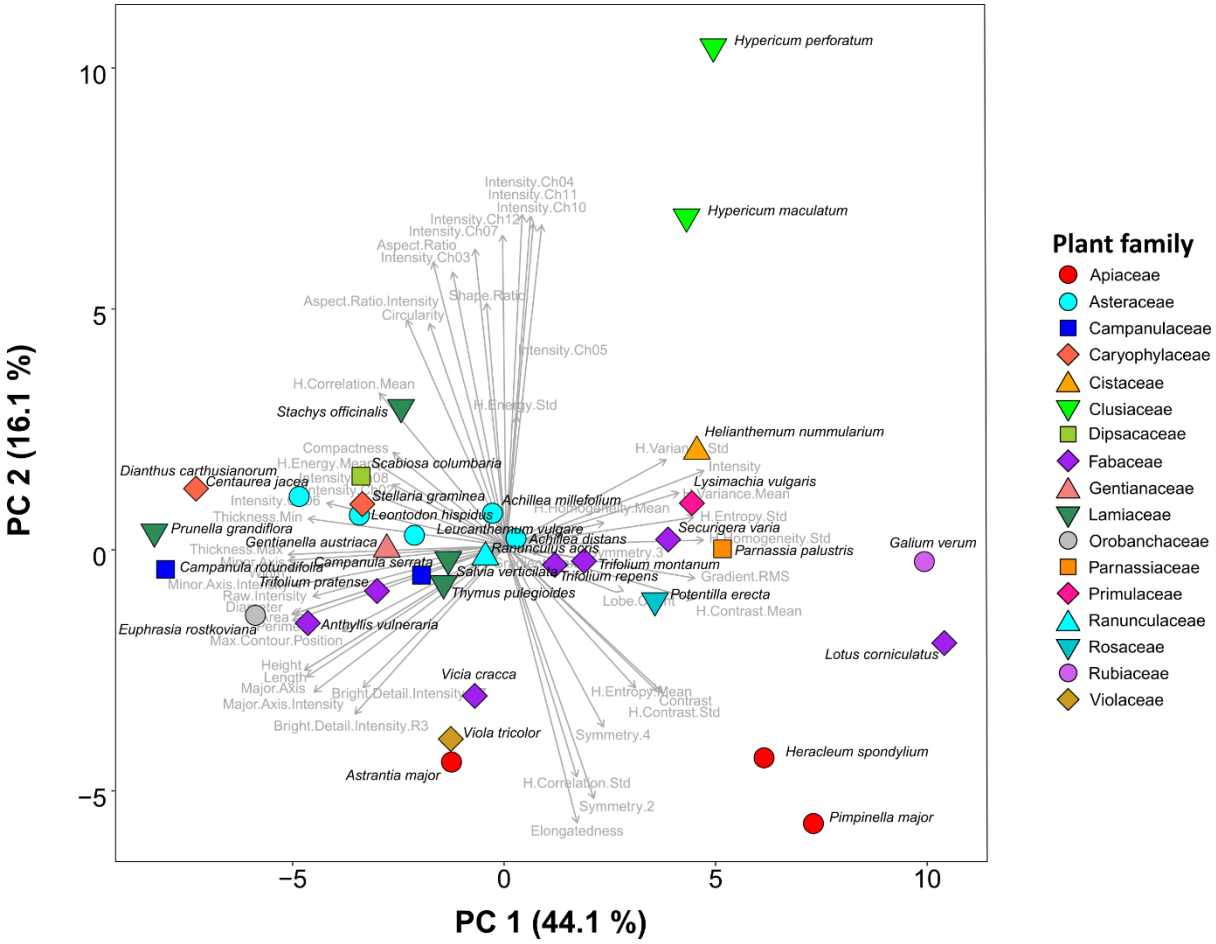

Fig. S3: Multiparameter comparison with Kruskal-Wallis-Test (paired) for testing differences of F-measure between channels (worst fluorescence channel 5, brightfield channel 9 and best multichannel comparison 7-9-2).

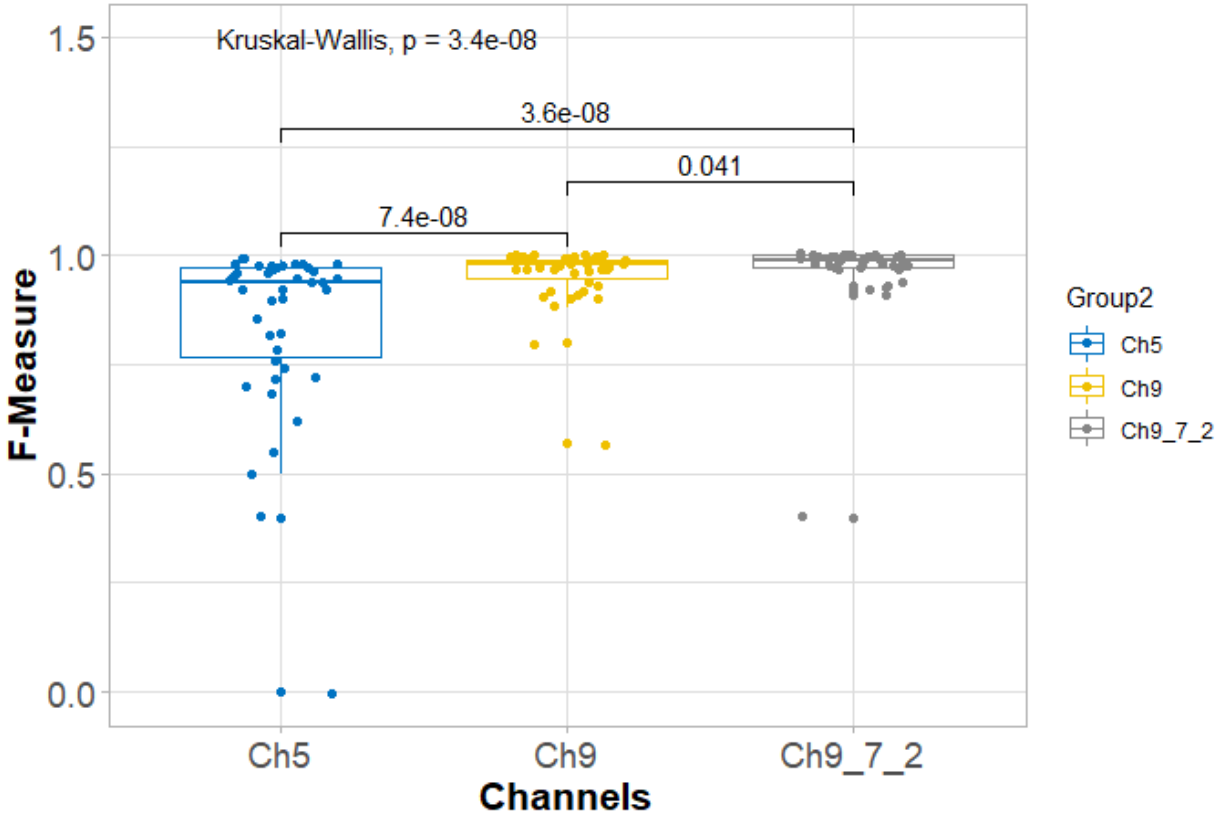

Fig. S4: Detailed figure in addition to Fig. 2, F-Measure for species (red & black) and plant family (orange & grey) level in relation to the log scaled number of measured pollen (sample size) available as reference data for the best multichannel classifier (channel 9-7-2, grey & black) and the worst single channel classifier (channel 5, orange & red). The arrows indicate some examples for the improvement of the F-Measure through the multi-channel classifier. Horizontal and vertical lines are shown for better orientation.

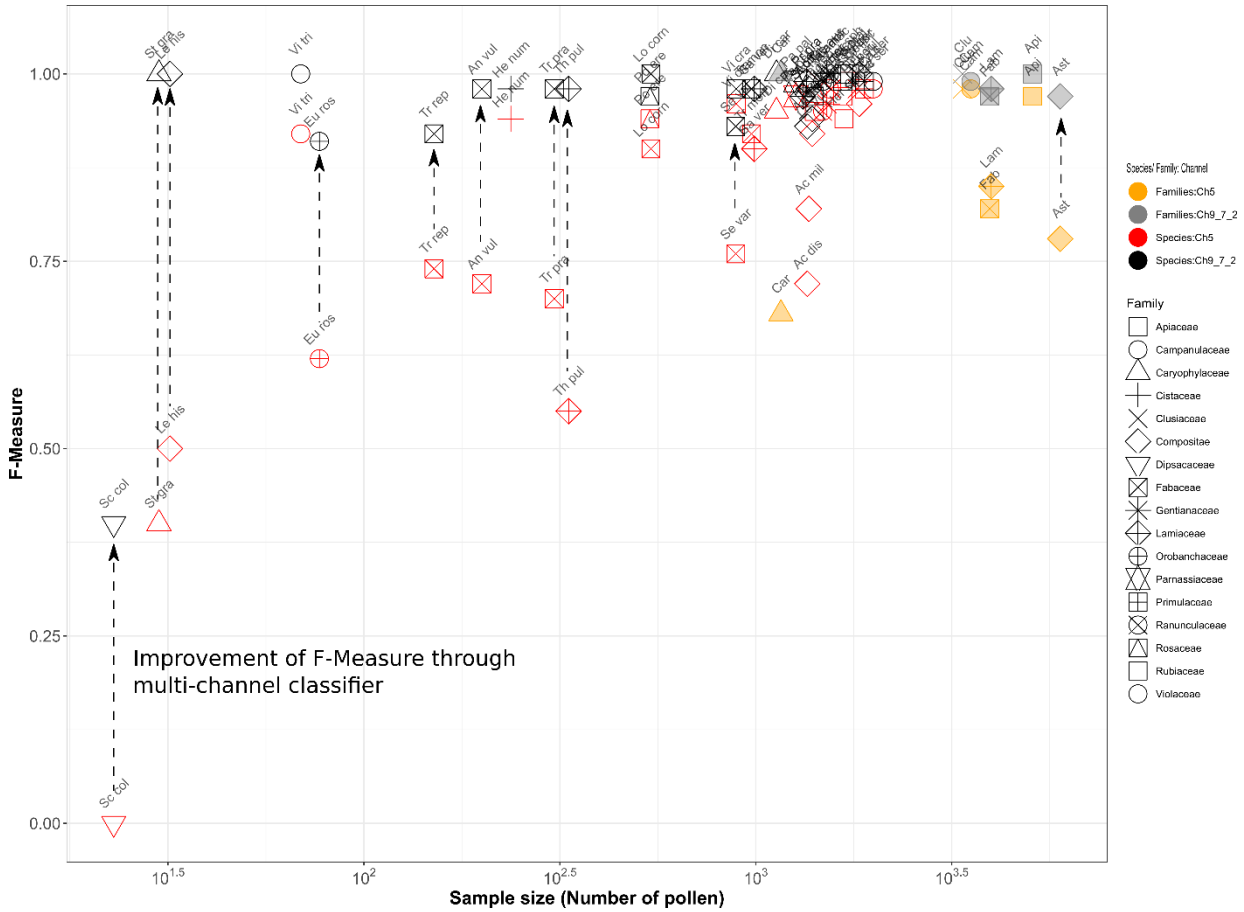

Supplemental tables

Table S1: Updated literature review based on the publication of (Holt & Bennett, 2014), covering literature from 2014 onwards[1].

	Classes (Species)	**Total number of images**	**Classification**	**Accuracy**
(Daood *et al.*, 2016)	30	1,060	Multi-layer feature decomposition	86.9 %
(Daood *et al.*, 2018)	10	3,920	CNN, RNN	100 %
(Marcos *et al.*, 2015)	15	1,800 (BF)	Multivariate analysis, KNN	94.8 %
(Khanzhina *et al.*, 2018)	11	1,774 (BF)	CNN	95.9 %
(Oteros *et al.*, 2015)		46,000 (BF)	Feature extraction	93.3 %
(Pedersen *et al.*, 2017)	31	13,617 (DF)	Feature extraction	93 %
(He *et al.*, 2019)		650 (BF)	Unsupervised	
(Arias *et al.*, 2017)	7/ 23	630/ 805	Feature extraction (GLCM)	96 %/ 79 %
(Sevillano & Aznarte, 2018)	23	805	CNN	97 %
(Sevillano *et al.*, 2020)	46	19,500	CNN (Alexnet)	98 %

[1] CNN – Convolutional Neural Network, RNN - Recurrent Neural Network, KNN – *k*-nearest neighbor, GLCM - gray-level co-occurrence matrices, BF – Brightfield, DF - Darkfield

Table S2: List of traits and their phylogenetic signal (p-values for Blomberg's K and Pagel's lambda). The traits are common features of image analysis (https://en.wikipedia.org/wiki/Shape_factor_(image_analysis_and_microscopy), and their formulas and explanations can be found elsewhere, e.g. for shape (Igathinathane *et al.*, 2008) or texture (Zhao *et al.*, 2014; Armi & Fekri-Ershad, 2019).

Traits	Blomberg's K	Pagel's lambda
Area	0.164	1.00
Aspect.Ratio	0.024	2.10E-03
Aspect.Ratio.Intensity	0.003	6.11E+09
Bright.Detail.Intensity.R3	0.121	1.00
Bright.Detail.Intensity.R7	0.022	0.08
Circularity	0.008	0.04
Compactness	0.020	0.09
Contrast	0.274	1.00
Diameter	0.135	1.00
Elongatedness	0.020	3.10E-04
Gradient.Max	0.011	1.54E-03
Gradient.RMS	0.047	0.03
H.Contrast.Mean	0.102	1.00
H.Contrast.Std	0.152	1.00
H.Correlation.Mean	0.152	1.00
H.Correlation.Std	0.048	1.00
H.Energy.Mean	0.118	0.12
H.Energy.Std	0.046	7.15E-04
H.Entropy.Mean	0.058	0.06
H.Entropy.Std	0.145	0.34
H.Homogeneity.Mean	0.006	0.04
H.Homogeneity.Std	0.214	0.42
H.Variance.Mean	0.096	1.00
H.Variance.Std	0.089	0.44
Height	0.123	1.00

Intensity	0.039	0.04
Intensity_MC_Ch02	0.092	0.07
Intensity_MC_Ch03	0.008	3.86E-03
Intensity_MC_Ch04	0.005	1.39E+05
Intensity_MC_Ch05	0.005	1.84E+05
Intensity_MC_Ch06	0.016	0.03
Intensity_MC_Ch07	0.009	5.16E+08
Intensity_MC_Ch08	0.060	0.78
Intensity_MC_Ch09	0.030	0.02
Intensity_MC_Ch10	0.003	1.43E+02
Intensity_MC_Ch11	0.003	3.18E+03
Intensity_MC_Ch12	0.008	6.27E+06
Length	0.120	1.00
Lobe.Count	0.001	3.87E+09
Major.Axis	0.138	1.00
Major.Axis.Intensity	0.057	1.00
Max.Contour.Position	0.011	0.01
Minor.Axis	0.145	1.00
Minor.Axis.Intensity	0.071	0.38
Perimeter	0.141	1.00
Raw.Intensity	0.202	1.00
Shape.Ratio	0.029	0.32
Symmetry.2	0.010	9.70E+09
Symmetry.3	0.001	2.81E-04
Symmetry.4	0.001	3.36E+07
Thickness.Max	0.131	0.57
Thickness.Min	0.046	0.14
Width	0.149	1.00
Intensity_MC_Ch01	0.179	0.03

References

Arias DG, Mussel Cirne MV, Chire JE, Pedrini H. 2017. Classification of Pollen Grain Images Based on an Ensemble of Classifiers. In: Chen X-w, ed. *16th IEEE International Conference on Machine Learning and Applications*. *ICMLA 2017 : 18-21 December 2017, Cancun, Mexico : proceedings*. Piscataway, NJ: IEEE.

Armi L, Fekri-Ershad S. 2019. Texture image analysis and texture classification methods - A review. *International Online Journal of Image Processing and Pattern Recognition Vol. 2, No.1, pp. 1-29* **2**: 1–29.

Daood A, Ribeiro E, Bush M. 2016. Pollen Recognition Using Multi-Layer Feature Decomposition. In: *FLAIRS Conference*.

Daood A, Ribeiro E, Bush M. 2018. Sequential Recognition of Pollen Grain Z-Stacks by Combining CNN and RNN. In: *FLAIRS Conference*.

He P, Glowacki G, Gkantiragas A. 2019. Unsupervised Representations of Pollen in Bright-Field Microscopy.

Holt KA, Bennett KD. 2014. Principles and methods for automated palynology. *New Phytologist* **203**: 735–742.

Igathinathane C, Pordesimo LO, Columbus EP, Batchelor WD, Methuku SR. 2008. Shape identification and particles size distribution from basic shape parameters using ImageJ. *Computers and Electronics in Agriculture* **63**: 168–182.

Khanzhina N, Putin E, Filchenkov A, Zamyatina E. 2018. Pollen grain recognition using convolutional neural network. In: *ESANN*.

Marcos JV, Nava R, Cristóbal G, Redondo R, Escalante-Ramírez B, Bueno G, Déniz Ó, González-Porto A, Pardo C, Chung F *et al.* 2015. Automated pollen identification using microscopic imaging and texture analysis. *Micron* **68**: 36–46.

Oteros J, Pusch G, Weichenmeier I, Heimann U, Möller R, Röseler S, Traidl-Hoffmann C, Schmidt-Weber C, Buters JT. 2015. Automatic and Online Pollen Monitoring. *International Archives of Allergy and Immunology* **167**: 158–166.

Pedersen B, Bailey DG, Hodgson RM, Holt K, Marsland S. 2017. Model and feature selection for the classification of dark field pollen images using the classifynder system. In: *2017 International Conference on Image and Vision Computing New Zealand (IVCNZ)*. *4-6 Dec. 2017*. Piscataway, NJ: IEEE.

Sevillano V, Aznarte JL. 2018. Improving classification of pollen grain images of the POLEN23E dataset through three different applications of deep learning convolutional neural networks. *PLOS ONE* **13**: e0201807.

Sevillano V, Holt K, Aznarte JL. 2020. Precise automatic classification of 46 different pollen types with convolutional neural networks. *PLOS ONE* **15**: e0229751.

Zhao Q, Shi C-Z, Luo L-P. 2014. Role of the texture features of images in the diagnosis of solitary pulmonary nodules in different sizes. *Chinese Journal of Cancer Research* **26**: 451–458.